Matching and surface barrier effects of the flux-line lattice in superconducting films and multilayers

M. Ziese* and P. Esquinazi†
Lehrstuhl für Experimentalphysik V, Universität Bayreuth, D-95440 Bayreuth, Germany

P. Wagner‡ and H. Adrian§
Technische Hochschule Darmstadt, Institut für Festkörperphysik, Hochschulstraße 8, D-64289 Darmstadt, Germany

S. H. Brongersma and R. Griessen
Vrije Universiteit Amsterdam, Faculty of Physics and Astronomy, De Boelelaan 1081, 1081 HV Amsterdam, The Netherlands

(Received 7 November 1995)

The flux-line lattice dissipation and the pinning force of $Bi_2Sr_2CaCu_2O_8$ and $YBa_2Cu_3O_7$ films and a Nb/Cu multilayer are investigated with the vibrating reed technique. In magnetic fields oriented under a small angle with respect to the film surfaces the Bi-2:2:1:2 film shows a series of pronounced dissipation maxima at matching fields B_N in the irreversible region of the magnetic phase diagram. The Y-1:2:3 film shows tiny damping maxima, whereas no structure in the dissipation of the Nb/Cu multilayer is detected below the upper critical field. The comparison of the matching fields to an anisotropic London model shows that the dissipation maxima are caused by rearrangements of the flux-line lattice configuration due to interactions with the sample surface. The different behavior of the high-temperature superconductors and the Nb/Cu multilayer is understood by explicitly taking the surface barrier into account. Deviations from the surface induced commensurability of the flux-line lattice due to the intrinsic pinning are discussed. Our results indicate that pancake vortices in the Bi-2:2:1:2 film should be coupled below the irreversibility line and below magnetic fields $B_\perp \leqslant 0.5$ T perpendicular to the film surface.

I. INTRODUCTION

The structure of the flux-line lattice (FLL) parallel to a superconducting film with a thickness d_p of the order of the penetration depth λ differs from the FLL in the thermodynamic limit in a bulk sample. Due to the interaction of the flux lines with the film surfaces an anisotropic FLL is formed.[1] At well defined field values B_N, $N=1, 2, 3, \ldots$, which will be called matching fields, the FLL rearranges from a state of $N-1$ to N flux-line rows parallel to the film. The critical current density sustained by the surface exhibits minima at the matching fields B_N.

The FLL parallel to a superconducting film has been studied by a variety of methods. The matching fields B_N have been determined in conventional superconductors by electron tunneling,[2] microwave absorption,[3] and resistivity measurements.[4–6] Pruymboom *et al.*[7] observed a periodic variation of the pinning force in 90 nm wide Nb_3Ge channels. Torque magnetization measurements on Nb/Cu multilayers show a series of maxima at field values B_N in the magnetization perpendicular to the layers.[8,9] The matching fields B_N are in agreement with results of Monte Carlo simulations of the flux-line positions in a superconducting film which were performed within the framework of the anisotropic London model.[8]

Hünnekes *et al.*[10] investigated the flux-line dissipation in $YBa_2Cu_3O_7$ films in magnetic fields parallel to the film surface with the vibrating reed technique. They observed a series of dissipation maxima in the irreversible region of the magnetic phase diagram which they interpreted as evidence for the matching of the FLL to the sample surfaces. Brongersma *et al.*[11] performed Monte Carlo simulations of the FLL in the Y-1:2:3 films using the anisotropic London model. However, in contrast to the situation in Nb/Cu multilayers the matching fields determined from the simulations are not in agreement with the experimentally observed field values at the flux-line dissipation maxima. The mechanism of the flux-line dissipation maxima in Y-1:2:3 films remained thus unclear.

In an attempt to understand the microscopic origin of the different behavior of $YBa_2Cu_3O_7$ and $Bi_2Sr_2CaCu_2O_8$ films on one side and Nb/Cu multilayers on the other side we investigate in this work the flux-line dissipation and pinning force of Bi-2:2:1:2 and Y-1:2:3 films and a Nb/Cu multilayer using the same experimental technique, i.e., the vibrating reed method. A major difference between these samples is their anisotropy factor $\gamma=\lambda_c/\lambda_{ab}$. λ_{ab} and λ_c denote the penetration depths for supercurrents flowing in the ab planes and along the c axis, respectively. Whereas the Nb/Cu multilayer is nearly isotropic with $\gamma\simeq 1.2$, the Y-1:2:3 film has an anisotropy constant[12] $\gamma\simeq 5$ and the Bi-2:2:1:2 film is highly anisotropic[13] $\gamma\simeq 150$.

The FLL in a Bi-2:2:1:2 film in a magnetic field at an angle Θ with respect to the sample plane can be described by a tilted stack of pancake vortices. From theory it is expected that only at very small angles $|\Theta| \ll \arctan(\gamma^{-1}) \simeq 0.4°$ between the magnetic field and the CuO_2 planes the vortex structure consists of pancake vortices connected by a lattice of Josephson vortices parallel to the superconducting planes.[14,15] It was verified experimentally that the dissipation

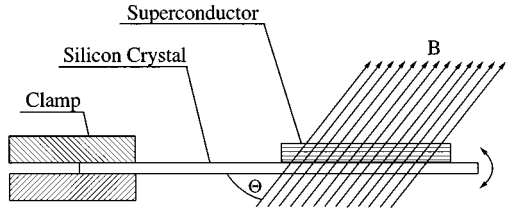

FIG. 1. Schematical setup of the vibrating reed. Θ denotes the angle between the external magnetic field and the film surface.

in high-T_c superconductors is mainly due to the motion of pancake vortices.[16–18] Therefore the measurement of the FLL structure and flux-line dissipation in magnetic fields slightly tilted with respect to the film surface provides information about the interaction between Josephson and pancake vortices and between individual pancake vortices. Our results indicate that the pancake vortices remain coupled in the field range $B \lesssim 6$ T and angle range $|\Theta| \lesssim 15°$, where we observe matching effects.

The paper is organized as follows. In the next section the experimental setup and sample preparation are briefly summarized. In Sec. III the experimental results for the Bi-2:2:1:2 and Y-1:2:3 films and for the Nb/Cu multilayer are presented. The interpretation is discussed in Sec. IV. The main conclusions are summarized in Sec. V.

II. EXPERIMENTAL DETAILS

In this work the flux-line lattice pinning and dissipation in superconducting films is studied with the vibrating reed technique. The films and their substrates are glued to silicon crystals with typical dimensions $l \times w \times d = 6.5 \times 2.0 \times 0.2$ mm^3. To drive the vibrating reed and detect its motion capacitively a thin silver layer of thickness ~ 10 nm is sputtered on the silicon crystals. A schematic drawing of the vibrating reed arrangement is shown in Fig. 1. An external static magnetic field B is applied at an angle Θ with respect to the film surface. The vibration amplitudes are of the order $\simeq 10$ nm.

The sample holder can be rotated *in situ* with an angular resolution $\Delta\Theta \simeq 0.01°$. The resonance frequency of the vibrating reed with the superconducting film glued to it is $\nu_0 \sim 5$ kHz in zero field and the quality factor in zero field is $Q_0 = \nu_0 / \Delta\nu_0 \sim 10^4$ at $T \lesssim 70$ K. $\Delta\nu_0$ denotes the half width of the resonance curve. The resonance frequency $\omega = 2\pi\nu$ and the inverse quality factor $Q_{\rm tot}^{-1}$ of the whole system are measured as a function of magnetic field B, angle Θ and temperature T. To obtain the inverse quality factor Q^{-1} of the superconducting film, $Q_{\rm tot}^{-1}$ is corrected for the zero field value Q_0^{-1}. The corrected inverse quality factor (or internal friction) $Q^{-1} \equiv Q_{\rm tot}^{-1} - Q_0^{-1}$ is in the following frequently called damping.

We investigated two high-temperature superconductor films, namely a Bi-2:2:1:2 and a Y-1:2:3 film, and a Nb/Cu multilayer.

The $Bi_2Sr_2CaCu_2O_8$ film was fabricated at the Technische Hochschule Darmstadt by dc sputtering onto a $SrTiO_3$ substrate. The thickness of the c-axis oriented film is $d_p = 320$ nm. The inductively measured critical temperature is $T_c = 89$ K with a transition width $\Delta T = 1.0$ K. From the 10×10 mm^2 film three pieces called BF1, BF2, and BF3 were cut with a diamond saw. These parts have the dimensions $l_p \times w_p = 2.20 \times 1.25$ mm^2 (BF1), $l_p \times w_p = 2.70 \times 1.35$ mm^2 (BF2), and $l_p \times w_p = 2.80 \times 0.85$ mm^2 (BF3). Further details on the preparation and characterization of the Bi-2:2:1:2 film can be found in Ref. 19.

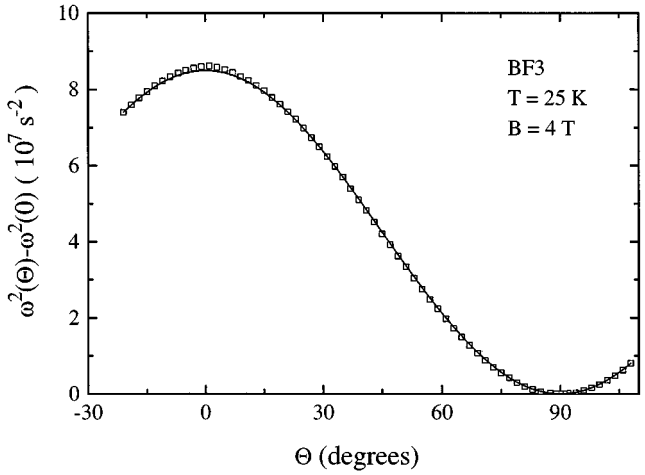

FIG. 2. Resonance frequency enhancement of Bi-2:2:1:2 film BF3 at $T = 25$ K and $B = 4$ T as a function of the angle Θ between the magnetic field and the film surface. The solid line is a fit of Eq. (1) to the data.

The 200 nm thin $YBa_2Cu_3O_7$ film was made at the A.F. Ioffe Physical-Technical-Institute, St. Petersburg. It was deposited on a $KTaO_3$ substrate by magnetron sputtering. The c axis is oriented perpendicular to the substrate. Details on the preparation and characterization of this film are described in Ref. 20. The measurements were performed on a part with dimensions $l_p = 2.2$ mm, $w_p = 1.6$ mm which was cut from the center of the film.

The Nb/Cu multilayer was deposited at the Vrije Universiteit in Amsterdam. It consists of 19 niobium layers of thickness 10 nm that are separated by 10 nm copper layers. The outer Nb layers were covered with 50 nm Cu layers to prevent the nucleation of surface superconductivity. The multilayer was grown on a sapphire substrate in a two-electron-gun UHV evaporation chamber. The resistively measured critical temperature is $T_c = 6$ K. Further information on the characterization of the Nb/Cu multilayer is found in Refs. 8 and 9. Magnetic moment measurements were performed on a multilayer strip of dimensions $l_p = 10$ mm and $w_p = 0.7$ mm using a torquemeter with a resolution of 10^{-9} Nm. The vibrating reed measurements were performed on a multilayer with dimensions $l_p = 2.7$ mm and $w_p = 0.7$ mm.

III. EXPERIMENTAL RESULTS

A. $Bi_2Sr_2CaCu_2O_8$ film

In this section the resonance frequency change and the damping of the Bi-2:2:1:2 films BF1, BF2, and BF3 in a magnetic field are presented.

In Fig. 2 the squared resonance frequency difference $\Delta\omega^2 \equiv \omega^2(B) - \omega^2(0)$ of sample BF3 is shown as a function of angle in a magnetic field $B = 4$ T at $T = 25$ K. $\Delta\omega^2$ is

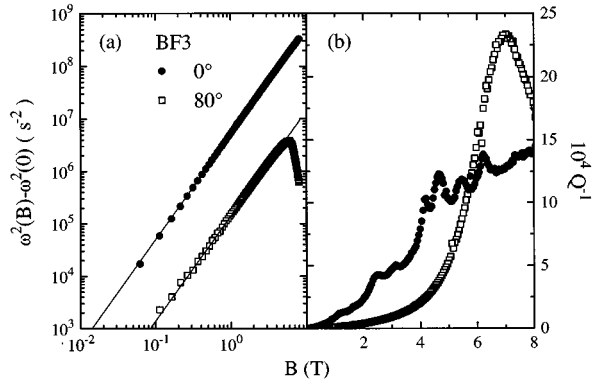

FIG. 3. (a) $\Delta\omega^2$ and (b) Q^{-1} of the Bi-2:2:1:2 film BF3 at $T=30$ K, $\Theta=0°$ and $\Theta=80°$. The solid lines in (a) are calculated with Eq. (1).

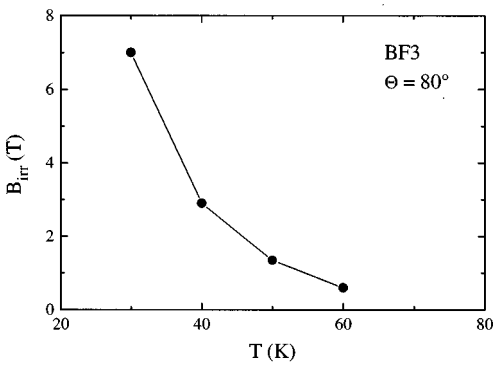

FIG. 4. Depinning line of the film BF3 at $\Theta=80°$. B_{irr} denotes the irreversibility field defined by the single damping maximum at $\Theta=80°$.

maximal for magnetic fields parallel to the film surface. The resonance frequency enhancement is mainly due to the shielding currents in the CuO_2 planes and is given by[21]

$$\omega^2(B)-\omega^2(0)=\omega_i^2-\omega_{\rm pin}^2-\Gamma^2, \tag{1}$$

with $\omega_i^2=(V_p/I)(\pi w_p/4d_p)(B^2/\mu_0)\cos^2\Theta$. V_p denotes the volume, w_p the width and d_p the thickness of the film. I is the effective moment of inertia of the silicon crystal with the substrate glued to it. The first term ω_i^2 on the right hand side of Eq. (1) is the ideal resonance frequency enhancement in the case of infinitely strong pinning, the second term $\omega_{\rm pin}^2$ accounts for corrections due to the finite pinning strength. $\omega_{\rm pin}^2$ is inversely proportional to the Labusch parameter[22,23] α. The third term on the right hand side of Eq. (1) is a correction term due to the damping $\Gamma=Q^{-1}\omega/2$. The correction terms are generally small and can be neglected in a first approximation.[24]

The solid line in Fig. 2 is a fit of Eq. (1) to the data with an effective moment of inertia $I=238\times10^{-12}$ kg m^2. The pinning correction and the damping are neglected. From the fit the absolute orientation of the magnetic field with respect to the film surface is determined with an accuracy $\Delta\Theta\lesssim0.5°$.

A comparison of $\Delta\omega^2$ and Q^{-1} at $\Theta=0°$ and $\Theta=80°$ is shown in Figs. 3(a) and 3(b). The measurements were performed in decreasing fields, after field cooling the film BF3 from above T_c to the measuring temperature $T=30$ K in an applied field $B=8$ T. The damping at $\Theta=80°$ shows a single broad maximum at $B\simeq7$ T that is accompanied by the vanishing of the resonance frequency enhancement. Since the resonance frequency enhancement is a measure of the pinning strength, we conclude that the FLL depins above $B\simeq7$ T at $T=30$ K, $\Theta=80°$ and $\nu_0\sim5$ kHz.

The maximum in the damping defines the depinning line.[25,26] Figure 4(a) shows the depinning line at $\Theta=80°$ defined by the single damping maximum. The extracted depinning line is in agreement with depinning lines found for Bi-2:2:1:2 crystals.[17,27]

In the following we turn to the discussion of the damping and resonance frequency change in a magnetic field oriented under a small angle with respect to the film surface. Figure 3(a) shows that $\Delta\omega^2$ at $\Theta=0°$ is monotonically increasing with increasing magnetic field $B\leqslant8$ T, i.e., at $\Theta=0°$, $T=30$ K and $B\leqslant8$ T the FLL is pinned. From Eq. (1) we expect $\Delta\omega^2\propto B^2$. The solid lines in Fig. 3(a) are calculated from Eq. (1) with the effective moment of inertia I obtained from the fit to the angle dependent resonance frequency change. They provide an excellent description of the data at $\Theta=0°$ in the complete magnetic field range and of the data at $\Theta=80°$ below the maximum in $\Delta\omega^2$.

Though the FLL is pinned at $\Theta=0°$, $T=30$ K and $B=8$ T a rich structure of maxima is seen in the damping at $\Theta=0°\pm0.5°$. Since the resonance frequency is continuously increasing with magnetic field, these maxima are *not* due to thermally activated depinning processes. Since they do not appear in the damping for large angles $|\Theta|>15°$, they are not due to second phases. Similar structures in the damping of vibrating Y-1:2:3 films have been reported by Hünnekes *et al.*[10] The mechanism leading to the structures in the damping Q^{-1} will be investigated in the following.

In Fig. 5 the damping of film BF2 is shown at $\Theta=5°$, 10 K $\leqslant T\leqslant$ 70 K on (a) a linear scale and (b) a semilogarithmic scale. For clarity the damping curves in (b) have been vertically displaced. As can be seen from Fig. 5(a) the structures in the damping at $T=30$ K and $T=50$ K are considerably smaller than the depinning peak which is measured at $T=70$ K. Note that the height of the damping maximum at the depinning line is related to the magnetic field by[28] $Q_{\rm max}^{-1}\propto B^2$. The structures in the damping below the irreversibility field $B_{\rm irr}$ might tentatively be related to a partial depinning of the FLL.

The peak structures in the damping at $T=30$ K and 50 K are similar in shape but the damping maxima at $T=50$ K are shifted to lower magnetic fields. To align the damping maxima in Fig. 5(b) the damping Q^{-1} is plotted versus a reduced field B/B^* with $B^*=1.0$ T for $T\leqslant30$ K and $B^*=0.87$ T for $T=50$ K, 60 K. Since the damping at $T=70$ K does not show any maxima below $B_{\rm irr}$ we arbitrarily choose $B^*=1$ T for $T=70$ K. As a function of the reduced field B/B^* the damping at different temperatures displays a series of maxima at the reduced fields indicated by the arrows. The damping maxima are most pronounced at 30 K $\leqslant T\leqslant$ 60 K, whereas they are washed out at low temperatures $T\leqslant20$ K and close to the irreversibility line at $T=70$ K. The meaning of the scaling field B^* is discussed in Sec. IV B.

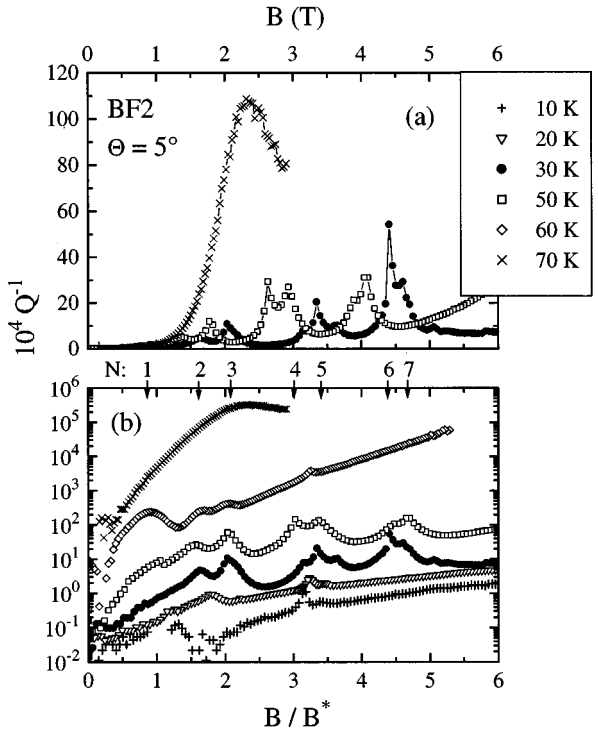

FIG. 5. Damping Q^{-1} of Bi-2:2:1:2 film BF2 at $\Theta=5°$ and different temperatures on (a) a linear and (b) a semilogarithmic scale. For clarity only three damping curves are shown in (a). To show the peak positions clearly the damping curves in (b) are vertically shifted. The damping curves have been multiplied by the factors 1/3 (10 K), 2/3 (20 K), 1 (30 K), 5 (50 K), 300 (60 K), 3000 (70 K). B^* denotes a scaling field with $B^*=1$ T for $T\leqslant 30$ K and $T=70$ K and $B^*=0.87$ T at $T=50$ K, 60 K. The arrows indicate the matching fields B_N numbered by integer values $N=1,2,\ldots$.

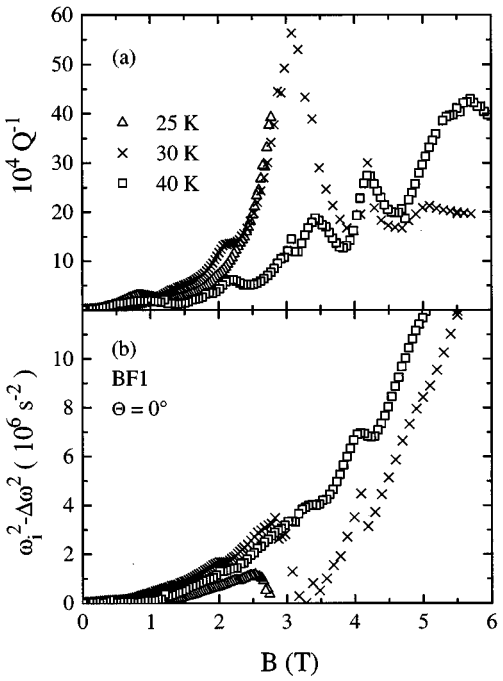

FIG. 6. (a) Damping Q^{-1} and (b) resonance frequency change $\omega_i^2-\Delta\omega^2$ of Bi-2:2:1:2 film BF1 at $\Theta=0°$. ω_i^2 denotes the resonance frequency enhancement due to the shielding currents in the superconducting planes in the limit of an infinite pinning force. Since $\Gamma^2\ll\omega_i^2-\Delta\omega^2$ the difference $\omega_i^2-\Delta\omega^2$ is proportional to the pinning correction $\omega_{\rm pin}^2\propto\alpha^{-1}$ [see Eq. (1)].

Angular dependent measurements show that the damping maxima in the irreversible regime of the B-T plane disappear for angles larger than $\Theta\sim 15°$.

The structures in the dissipation are correlated with anomalies in the pinning force. In Fig. 6(a) the damping Q^{-1} and (b) the squared resonance frequency change of the film BF1 are shown at $\Theta=0°$. From the measured resonance frequency enhancement $\Delta\omega^2$ the ideal resonance frequency change due to the shielding currents in the superconducting planes, see Eq. (1), is subtracted, i.e., the correction term $\omega_{\rm pin}^2\simeq\omega_i^2-\Delta\omega^2\propto\alpha^{-1}$ is displayed in Fig. 6(b). The anomalies in the resonance frequency enhancement, i.e., in the pinning force, are uniquely correlated with the dissipation maxima. Since $\Gamma^2\ll\omega_i^2-\Delta\omega^2$, the structures in the resonance frequency are not caused by the damping correction in Eq. (1) but are due to anomalies in the pinning correction term $\omega_{\rm pin}^2$.

B. $YBa_2Cu_3O_7$ film

The dissipation of the Y-1:2:3 film was measured in magnetic fields oriented under a small angle with respect to the film surface. In Fig. 7 the damping is shown at $\Theta=0°$ as a function of magnetic field for $T=20$ K and $T=70$ K. The field cooled measurements (FC) show small dissipation maxima at $B_1\simeq 0.45$ T and $B_2\simeq 0.9$ T; see inset to Fig. 7. In the ZFC measurement at $T=20$ K no dissipation maxima are observed. Further measurements in the temperature range 6 K $\leqslant T\leqslant$ 40 K and angle range $0°\leqslant\Theta\leqslant 5°$ showed no evidence for damping maxima in the irreversible regime of the magnetic phase diagram.

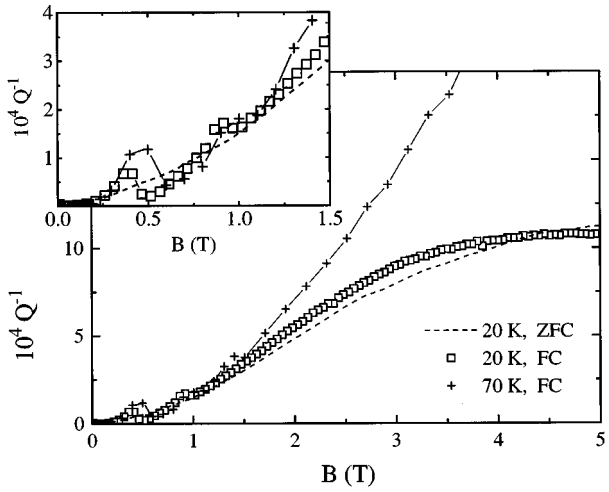

FIG. 7. Damping Q^{-1} of a 200 nm thin Y-1:2:3 film at $\Theta=0°$, $T=20$ K and $T=70$ K. The inset shows the damping at low magnetic fields. FC stands for field cooled and ZFC for zero field cooled.

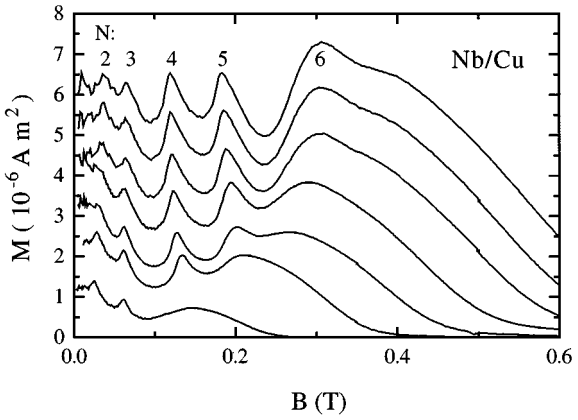

FIG. 8. Magnetic moment perpendicular to the Nb/Cu multilayer as a function of magnetic field applied under an angle $\Theta = 1°$ with respect to the layers. The temperatures are, from top to bottom, 2.2 K, 2.5 K, 2.9 K, 3.3 K, 3.7 K, 4.2 K, 5.0 K. The peaks are labeled by the number N.

C. Nb/Cu multilayer

The magnetic moment perpendicular to the Nb/Cu multilayer is shown in Fig. 8 for different temperatures 2.2 K $\leqslant T \leqslant$ 5.9 K. The magnetic field is applied under an angle $\Theta = 1°$ with respect to the layers. The magnetic moment shows a series of pronounced maxima. When the angle Θ between magnetic field and the layers is increased the height of the maxima in the magnetic moment gradually decreases and vanishes around $\Theta \sim 6°$. The position of the peaks is independent of temperature implying that the penetration length λ_{ab} is larger than the thickness of the sample, i.e., $\lambda_{ab} > d_p$.

The angular dependence of the squared resonance frequency difference of the Nb/Cu multilayer is shown in Fig. 9 at $T = 4.5$ K and $B = 0.4$ T. $\Delta\omega^2$ has a triangular shape with $\Delta\omega^2 = 0$ for $|\Theta| > 35°$.

The resonance frequency change and damping of the vibrating multilayer was measured as a function of magnetic field at constant angle $0° \leqslant \Theta \leqslant 8°$. In Figs. 10(a) and 10(b) $\Delta\omega^2$ is shown on a linear and a logarithmic scale, respectively. The solid line in 10(b) is a fit of Eq. (1) to the low field data with $I = 125 \times 10^{-12}$ kg m^2 neglecting the correction terms. In Figs. 10(c) and 10(d) the damping Q^{-1} is shown on a linear and a logarithmic scale. A damping maximum is seen at the upper critical field B_{c2} that is accompanied by the vanishing of the resonance frequency enhancement. Within the experimental resolution no structures in the dissipation can be resolved in the irreversible regime of the B-T plane.

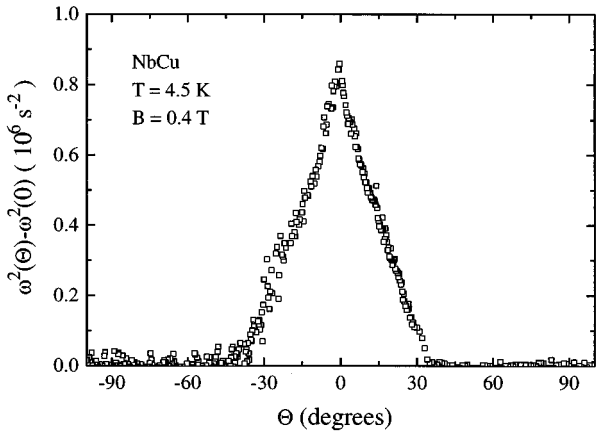

FIG. 9. Angular dependence of the resonance frequency enhancement of the Nb/Cu multilayer at $T = 4.5$ K and $B = 0.4$ T.

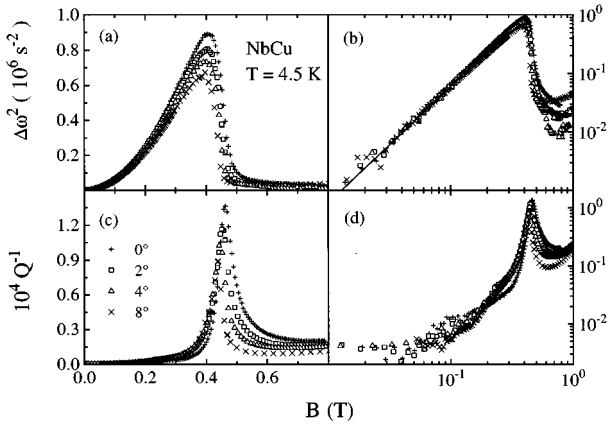

FIG. 10. Nb/Cu multilayer: (a), (b) $\Delta\omega^2$ and (c), (d) Q^{-1} as a function of magnetic field at $T = 4.5$ K. The solid line in (b) is a fit of Eq. (1) to the low field data.

From Fig. 10 we determine $B_{c2} = 0.48$ T at $T = 4.5$ K and $\Theta = 0°$. From the measurement of the angular dependent resonance frequency the anisotropy constant of the Nb/Cu multilayer can be estimated. Assuming $B_{c2}(90°) \leqslant B_{c2}(35°) = 0.4$ T at $T = 4.5$ K an anisotropy constant $\gamma = B_{c2}(0°)/B_{c2}(90°) \geqslant 1.2$ follows.

We stress that the vibrating reed measurements are performed at low effective ac magnetic field amplitudes $b_{ac} \sim 1\ \mu$T at $B = 0.1$ T.

IV. MODEL AND INTERPRETATION

The existence of a series of maxima in the dissipation of vibrating $Bi_2Sr_2CaCu_2O_8$ films has been shown in the preceding paragraph. Hünnekes *et al.*[10] observed a series of dissipation maxima in vibrating $YBa_2Cu_3O_7$ films, if the magnetic field is parallel to the film surfaces. The 200 nm thin Y-1:2:3 film investigated here showed only tiny dissipation maxima in the irreversible region of the magnetic phase diagram. A Nb/Cu multilayer showed no damping maxima below B_{c2}, but clear maxima in the irreversible magnetization were observed.

Since vibrating reed measurements on high-temperature *single crystals* of thickness $d_p > 50\ \mu$m much larger than the penetration depth λ_{ab} do not show any dissipation maxima below the irreversibility line,[21,24] we conclude that the observed dissipation maxima in the high-temperature *film* samples are related to the interaction of the flux-line lattice with the sample surface. The flux-line lattice in the superconducting films forms a configuration that is commensurate with the sample thickness. At the matching fields the flux-line configuration is supposed to become unstable and rearrange to another stable configuration. We shall show that the

seemingly conflicting results for the high-T_c films and the Nb/Cu multilayer can be consistently interpreted when the surface barrier is taken into account.

A. Flux-line lattice configuration in a superconducting film

A flux line near and parallel to the surface of a superconducting sample experiences two forces. The Lorentz force due to the interaction with the Meissner currents in a surface region of depth λ_{ab} is directed into the superconductor. The image force due to the interaction of the flux line with its image vortex is directed outwards. These forces lead to the appearance of surface barriers for the entry and exit of flux lines.[29,30]

The FLL parallel to a superconducting film with $d_p<\lambda_{ab}$ has been investigated by Carter,[31] Takács,[32] Brongersma *et al.*,[8] and Mawatari and Yamafuji.[1] These investigations were performed within London theory. In the following λ_{ab} and λ_c denote the penetration depths for supercurrents flowing in the ab planes and along the c axis, respectively, ξ_{ab} and ξ_c denote the coherence lengths in the CuO_2 planes and along the c axis. The anisotropy constant is defined as $\gamma=\lambda_c/\lambda_{ab}$.

Brongersma *et al.*[8] performed Monte Carlo simulations of the FLL parallel to a superconducting film with $d_p<\lambda_{ab}$ in the *absence* of a transport current. They observed the formation of N flux-line rows with a separation $A_x=d_p/(N+1)$, $N=2,3,\ldots$. The flux lines rearrange at well defined fields B_N from N to $N+1$ rows. The Monte Carlo simulations are performed with a fixed number of vortices in a layer of thickness d_p and length L. A varying vortex density is simulated by variation of L. Due to this simulation procedure the surface barrier for the entry of vortices in the superconducting film is neglected and the first row of vortices appears at the lower critical field

$$B_{c1}=\frac{2\Phi_0}{\pi\gamma d_p^2}\ln\left[\frac{\gamma d_p}{\xi_{ab}}\right]. \tag{2}$$

Φ_0 denotes the flux quantum. The reduced matching fields B_N/B_{c1} are dependent on the parameter $\xi_{ab}/\gamma d_p$. Brongersma *et al.*[8] showed that the rearrangements of the flux lines take place at the magnetic field values that correspond to the experimentally determined maxima in the magnetic moment perpendicular to the multilayer. From this result we conclude that surface barriers for flux-line entry and exit are negligible in the Nb/Cu multilayers. This may be due to the rather thick outer Cu layers evaporated on the multilayers.[8]

Mawatari and Yamafuji[1] investigated the FLL parallel to a superconducting film in the *presence* of a transport current J parallel to the film surface and perpendicular to the flux lines by explicitly taking into account that vortices had to cross the surface barrier. They analytically calculated the critical current density J_c sustained by the surface, the separation of the flux-line rows A_x and the flux-line lattice constant along the rows A_y. In this model surface barriers prove to be important and the field scale of the matching effect is the superheating field

$$B_{\rm sh}=\frac{\Phi_0}{\sqrt{2}\pi\xi_{ab}d_p}. \tag{3}$$

The superheating field is the maximal magnetic field value for which the Meissner state is stable. In a zero field cooled magnetization measurement without an applied transport current the surface barrier for vortex entry does not vanish for magnetic fields up to $B_{\rm sh}$.

For the investigated Bi-2:2:1:2 film we have $d_p=320$ nm, $\lambda_{ab}=200$ nm,[33] $\xi_{ab}\simeq 2.0$ nm,[34] and $\gamma\simeq 150$.[13] Therefore we get from Eq. (2) $B_{c1}\simeq 9\times10^{-4}$ T and from Eq. (3) $B_{\rm sh}\simeq 0.7$ T. The damping shows maxima at magnetic fields $B_N\geqslant 0.7$ T, i.e., the observed field scale for the occurence of the dissipation maxima is of the order of the superheating field $B_{\rm sh}$ and not of B_{c1}. Therefore we analyze the appearance of the dissipation maxima within the model of Mawatari and Yamafuji.[1]

The calculations are performed for a FLL parallel to the film surfaces since in this case the method of image vortices can be used. We expect the results to be qualitatively unchanged in the small angle range where surface pinning is strong.

We note that this model is valid for three-dimensional-(3D) anisotropic superconductors. Since Bi-2:2:1:2 films and crystals are strongly anisotropic, they should be described within the Lawrence-Doniach model.[35,36] However, Josephson strings connecting the pancake vortices nucleate only at very small angles[14,15] with $\cot\Theta\gg\gamma$. Using $\gamma\simeq 150$ we obtain $|\Theta|\ll 0.4°$. For larger angles the Lawrence-Doniach model is equivalent to the anisotropic London model. Since the misalignment angle in our measurements is $\Delta\Theta\simeq 0.5°$ we can interpret the results obtained on the Bi-2:2:1:2 films within the model of Mawatari and Yamafuji.[1]

Feinberg and Buzdin[37] estimated the superheating field of a *bulk* sample ($\lambda_{ab}\ll d_p$) in magnetic fields *parallel* to the layers in the Lawrence-Doniach model and obtained

$$B_{\rm sh\|}=\Phi_0/\pi\lambda_{ab}\gamma s \tag{4}$$

for $T<T^*$ and

$$B_{\rm sh\|}=\Phi_0/\sqrt{2}\pi\lambda_{ab}\xi_{ab} \tag{5}$$

for $T>T^*$. The crossover temperature T^* is defined by $\xi_c(T^*)=s/\sqrt{2}$. s denotes the layer separation. With $\lambda_{ab}\simeq 200$ nm, $\gamma\simeq 150$ and $s=1.5$ nm for Bi-2:2:1:2 one obtains $B_{\rm sh\|}(T\ll T^*)\simeq 0.01$ T. Since $B_{\rm sh\|}\ll B_{\rm sh}$ and since the matching fields are of the order of $B_{\rm sh}$ we conclude that the measurements were performed in an angle range where the Bi-2:2:1:2 film can be described by the anisotropic London theory.

B. $Bi_2Sr_2CaCu_2O_8$ film

In the Appendix the equations for the critical current density and the FLL constants derived by Mawatari and Yamafuji[1] are summarized. The field scale is the superheating field $B_{\rm sh}$ and the critical current density scale is the depairing current

$$J_{\rm dp}=\frac{\Phi_0}{2\sqrt{2}\pi\mu_0\gamma^{1/2}\lambda_{ab}^2\xi_{ab}}. \tag{6}$$

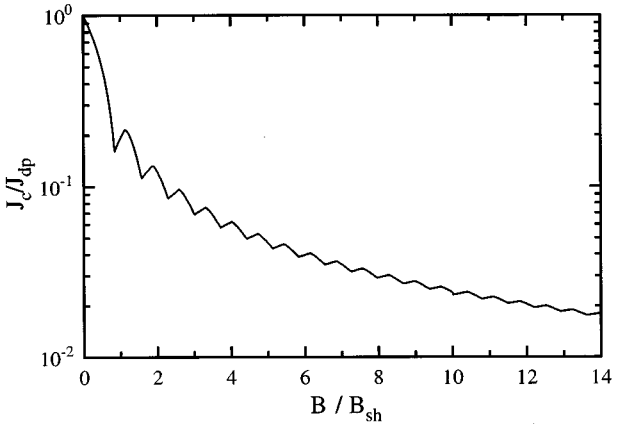

FIG. 11. Theoretical critical current density J_c/J_{dp} of a superconducting film in a parallel magnetic field. J_c is calculated in the limit $\xi_{ab}/\gamma d_p \ll 1$. The critical current density is minimal at magnetic fields B_N, where the FLL undergoes a rearrangement from $N-1$ to N flux-line rows.

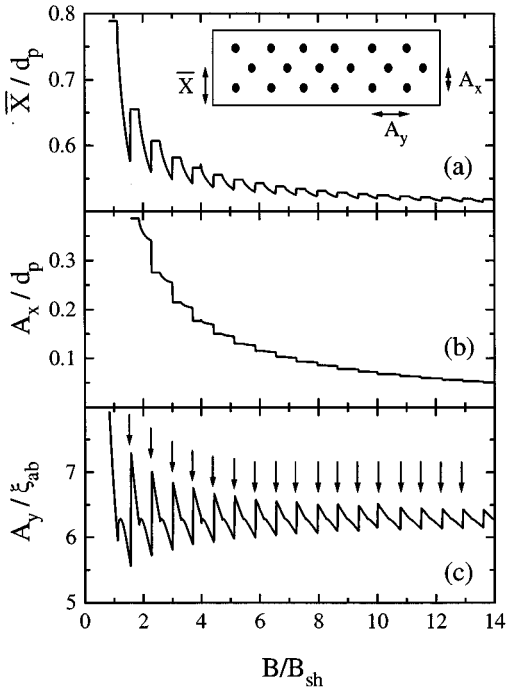

FIG. 12. (a) Averaged position $\bar{X}$ of the flux-line rows and (b) separation A_x of the flux-line rows along the thickness of the superconducting film. (c) Flux-line row constant A_y. The inset to (a) shows a schematic picture of the flux-line configuration. $\bar{X}$, A_x, and A_y are calculated in the limit $\xi_{ab}/\gamma d_p \ll 1$ in the presence of the critical transport current perpendicular to $\vec{B}$ and parallel to the film surface that is shown in Fig. 11. The arrows in (c) mark the fields B_N, where rearrangements of the FLL take place. Note that due to the presence of the transport current vortices nucleate in the film already below B_{sh}.

The single parameter in the theory is the ratio $\xi_{ab}/\gamma d_p$. With typical superconducting parameters of Bi-2:2:1:2 samples we obtain $\xi_{ab}/\gamma d_p < 10^{-3}$.

In the Appendix we derive the equations for the FLL configuration in the first order in $\xi_{ab}/\gamma d_p$, which is an excellent approximation for $\xi_{ab}/\gamma d_p < 10^{-3}$ and $N \leqslant 20$.

In Fig. 11 the reduced critical current density J_c/J_{dp} with $J_{\mathrm{dp}} \simeq 2\times 10^{11}$ A/m^2 is shown as a function of the reduced field B/B_{sh}. The critical current density is calculated with Eqs. (A2)–(A15). J_c has a nonmonotonous behavior. The minima in J_c at fields B_N occur whenever the FLL rearranges from $N-1$ to N rows. In Fig. 12 we show the average position $\bar{X}$ of the flux-line rows along the film thickness and the flux lattice constants A_x along the thickness and A_y along the rows as a function of the magnetic field B. The values of $\bar{X}$, A_x and A_y displayed in Fig. 12 are calculated for a transport current density equal to the critical current density J_c sustained by the surface barriers. A_y exhibits a sawtooth structure that clearly marks the rearrangements of the vortex lattice.

The interaction of the FLL with the film surface creates an anisotropic FLL with $A_x \simeq 56$ nm and $A_y \simeq 12.5$ nm for the Bi-2:2:1:2 film at $B = 4B_{\mathrm{sh}} \simeq 2.4$ T. The anisotropic FLL is stabilized by the long range interaction between the flux lines and between the flux lines and the film surface. The influence of the sample surfaces on the flux-line configuration becomes particularly clear if we compare the FLL constants A_x and A_y to their corresponding values a_c and a_{ab} in *bulk samples*. Magnetic fields parallel to the *ab* planes of a *bulk* sample create an anisotropic FLL with lattice constants $a_{ab} = (\gamma\Phi_0/B)^{1/2}$ parallel to the superconducting planes and $a_c = (\Phi_0/\gamma B)^{1/2}$ perpendicular to the planes. For Bi-2:2:1:2 samples with an anisotropy constant $\gamma \simeq 150$ we obtain the lattice constants $a_{ab} \simeq 360$ nm and $a_c \simeq 2.4$ nm in a field $B = 4B_{\mathrm{sh}} \simeq 2.4$ T, i.e., in this case is $a_{ab} \gg a_c$.

The arrows in Fig. 12(c) mark the matching fields B_N. The matching fields determined either from the discontinuities in A_y or by the minima in J_c agree and are plotted in Fig. 13 as a function of the flux-line row number N. In the limit $\xi_{ab}/\gamma d_p \ll 1$ the fields B_N depend linearly on N according to

$$B_N = B_{\mathrm{sh}}(0.19 + 0.71N). \tag{7}$$

For the Bi-2:2:1:2 film we obtain $\Delta B = B_{N+1} - B_N = 0.71B_{\mathrm{sh}} \simeq 0.5$ T with a superheating field for an anisotropic superconductor $B_{\mathrm{sh}} = 0.7$ T.

In order to compare the theory to the data we have numbered the matching fields as indicated in Fig. 5. For temperatures $T \leqslant 40$ K no temperature dependence of the matching fields could be detected, for larger temperatures the damping maxima shift to smaller magnetic fields. This is in qualitative agreement with Eq. (7). It was not possible to determine the temperature dependence of the phenomenologically introduced scaling field $B^* \propto B_{\mathrm{sh}}$. Furthermore not all expected matching fields are observed. These deviations from the theory will be discussed later.

In Fig. 14 the matching fields of the three parts of the Bi-2:2:1:2 film (a) BF1, (b) BF2, and (c) BF3 are shown at $\Theta = 0° \pm 0.5°$. The matching fields show a linear dependence on the number of flux-line rows N with slopes $\Delta B = 0.68$ T for BF1 and BF2 and $\Delta B = 0.75$ T for BF3. The matching fields of film BF2 at $\Theta = 5°$ are shown in Fig. 15. The sepa-

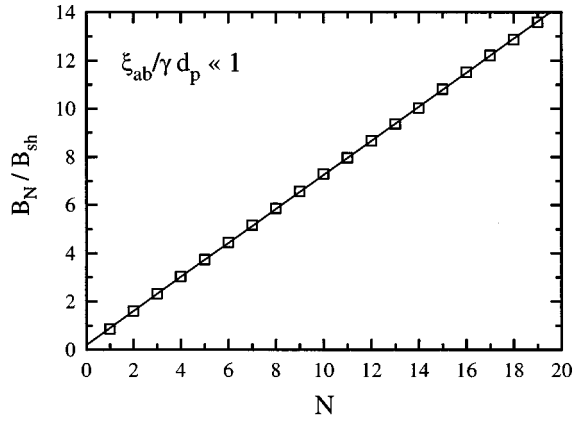

FIG. 13. Calculated matching fields B_N in the limit $\xi_{ab}/\gamma d_p \ll 1$. The matching fields are defined by the minima in the critical current density or equivalently by the jumps in the lattice constant A_y. The solid line is the function $B_N = B_{sh}(0.19 + 0.71N)$.

ration between two matching fields is $\Delta B = 0.66$ T at $\Theta = 5°$, i.e., the slope ΔB is independent of angle for $|\Theta| \leq 5°$.

The slopes $\Delta B = 0.7 \pm 0.1$ T determined at $\Theta = 0°$ and $\Theta = 5°$ are in good agreement with the theoretical estimate $\Delta B \simeq 0.5$ T for a thin anisotropic superconducting film. Therefore the fundamental mechanism causing the FLL dissipation maxima in the irreversible region of the magnetic phase diagram is the rearrangement of the flux lines at small angles to the film plane. The deviations from the theoretical

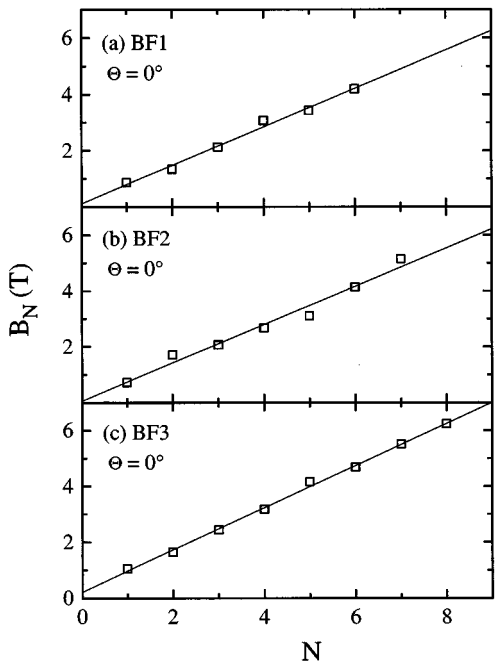

FIG. 14. Experimentally determined matching fields of the Bi-2:2:1:2 films (a) BF1, (b) BF2, and (c) BF3 as a function of the flux-line row number N. The angle between the magnetic field and the film surface is $\Theta = 0° \pm 0.5°$. The matching fields are determined for temperatures 20 K $\leq T \leq$ 40 K.

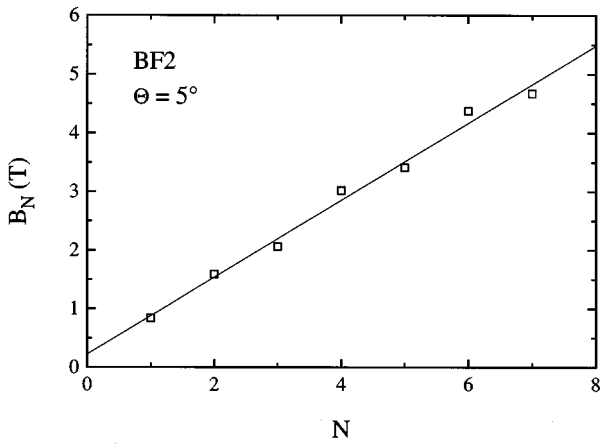

FIG. 15. Matching fields of Bi-2:2:1:2 film BF2 at $\Theta = 5°$ and 10 K $\leq T \leq$ 60 K.

estimate might be attributed to the surface roughness and to the crudeness of that estimate.

The FLL at $\Theta = 5°$ consists of tilted stacks of pancake vortices. From the angle independence of the matching fields we conclude that the dissipation and matching effects in the whole investigated angle range are due to pancake vortices. These stacks of pancakes must be coupled in the investigated field $B \leq 6$ T and angle $|\Theta| \leq 5°$ range, i.e., for magnetic fields $B_\perp \leq 0.5$ T perpendicular to the CuO_2 planes. Our results indicate that the superheating field B_{sh} of a stack of pancake vortices is of the same order of magnitude as the superheating field of a flux line in a 3D-anisotropic superconducting film.

Since the matching effects are not observed for angles larger than $\Theta \sim 15°$ we conclude that surface barriers are not important for $|\Theta| \gtrsim 15°$. This is similar to angle dependent measurements of the critical current density in NbTa films[38] which show that surface pinning is effective in an angle range $|\Theta| \lesssim 15°$.

Before discussing deviations from the model we turn to the interpretation of the data obtained for the Y-1:2:3 film and the Nb/Cu multilayer.

C. $YBa_2Cu_3O_7$ film

The 200 nm thin Y-1:2:3 film investigated in this work has the parameters $B_{sh} \simeq 1.5$ T, $B_{c1} \simeq 10$ mT, and $\xi_{ab}/\gamma d_p \simeq 10^{-3}$. We have used the values $\xi_{ab} \simeq 15$ nm and $\gamma \simeq 5$. Therefore the first damping maxima are expected from Eq. (7) at the fields $B_1 \simeq 1.35$ T and $B_2 \simeq 2.4$ T. We measured tiny maxima in the damping at $B_1 \simeq 0.45$ T and $B_2 \simeq 0.9$ T. The reduced matching fields can be understood assuming a value for the superheating field that is reduced to one third of the theoretical value.

In the following we shortly discuss the results of Hünnekes *et al.*[10,39] who measured the damping of vibrating Y-1:2:3 films with a thickness in the range 43 nm $\leq d_p \leq$ 600 nm. All investigated films showed a series of damping maxima as a function of the applied magnetic field $B \leq 2.5$ T. The measurements were carried out at $T = 20$ K. The positions of the damping maxima of a 43 nm and a 275 nm thin

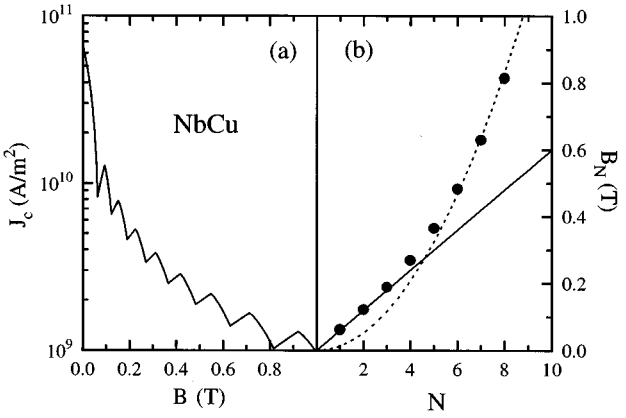

FIG. 16. (a) Theoretical critical current density J_c in a parallel magnetic field calculated with the supercondcuting parameters of the Nb/Cu multilayer. (b) Matching fields determined from the minima in J_c. For small N a linear dependence $B_N \propto N$ is found (solid line), for large N a quadratic dependence $B_N \propto N^2$ is seen (dotted line).

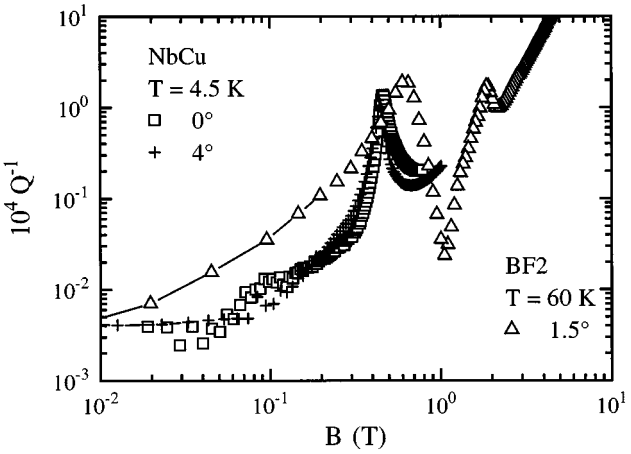

FIG. 17. Comparison of the damping Q^{-1} of the Nb/Cu multilayer at $T=4.5$ K, $\Theta=0°$ and $\Theta=4°$ and the damping of the Bi-2:2:1:2 film BF2 at $T=60$ K, $\Theta=1.5°$.

film were also measured at 50 K and 80 K, respectively. The matching fields were only weakly shifted by temperature.

Except for the 43 nm thin film the results for all films investigated by Hünnekes *et al.*[10,39] can be qualitatively understood if surface barriers are taken into account. However, the experimentally determined superheating fields of the Y-1:2:3 films are lower than the calculated values. The reduction of the superheating fields might be attributed to surface roughness.

The 43 nm thin Y-1:2:3 film investigated by Hünnekes *et al.*[10] exhibits matching fields $B_1=0.25$ T and $B_2=0.8$ T. Brongersma *et al.*[11] pointed out that the calculated lower critical field parallel to the CuO_2 planes $B_{c1}=0.56$ T is higher than the first matching field. Due to this fact and the limited experimental resolution[40] of the damping measurement the data for the 43 nm film are not conclusive with regard to a comparison with the theory.

D. Nb/Cu multilayer

The Nb/Cu multilayer has the parameters $\xi_{ab}=16$ nm and $\gamma \simeq 1.2$. With an effective thickness $d_p \simeq 400$ nm we obtain $J_{\mathrm{dp}} \simeq 6.6\times 10^{10}$ A/m^2, $B_{\mathrm{sh}} \simeq 0.072$ T, and $\xi_{ab}/\gamma d_p \simeq 0.036$. Figure 16(a) shows the calculated critical current density. The matching fields B_N determined from the minima in the critical current density are shown in Fig. 16(b) (●). For small flux-line row numbers N the matching field B_N is linear in N [solid line in Fig. 16(b)], whereas $B_N \propto N^2$ is found for large N [dotted line in Fig. 16(b)].

In the experimentally accessible field range $B<0.4$ T at $T=4.5$ K five dissipation maxima are expected from the theoretical calculations presented in Fig. 16(b) but are not observed experimentally. However, the magnetization perpendicular to the multilayers indeed shows four maxima at $T=4.2$ K. The experimentally determined matching fields are $B_N=0.028$, 0.060, 0.131, 0.21 T, $N=1$, 2, 3, 4. Taking into account the uncertainty in the thickness of the multilayer that originates from the 50 nm outer copper layers the experimentally determined fields are in excellent agreement with the calculated rearrangement fields $B_N=0.024$, 0.058, 0.122, 0.185 T, $N=1$, 2, 3, 4, obtained from the Monte Carlo simulations.[41] However, the rearrangement fields $B_N=0.060$, 0.119, 0.188, 0.268 T, $N=1$, 2, 3, 4, obtained from the model of Mawatari and Yamafuji[1] are significantly larger than the matching fields determined from the torque magnetization. This comparison proves that surface barriers for the entry of vortices in the multilayer are not effective. This is consistent with measurements of the critical current density due to surface pinning that is reduced in superconductors plated with a normal metal.[42] Furthermore graded Ta/NbTa/Ta films with a smooth interface between the Ta and the NbTa layers show strongly reduced surface pinning.[38]

Why are maxima not observed in the dissipation of the Nb/Cu multilayer? One possibility might be that the sensitivity of the vibrating reed technique is not sufficient. To check this we compare the damping Q^{-1} of the Bi-2:2:1:2 film BF2 at $T=60$ K, $\Theta=1.5°$ and of the Nb/Cu multilayer at $T=4.5$ K, $\Theta=0°$ and $\Theta=4°$ in Fig. 17. The flux-line dissipation in the Bi-2:2:1:2 film at the matching fields is larger than the dissipation in the multilayer at the transition to the normal state. From this comparison we conclude that the dissipation level at the matching fields should be well above the experimental resolution if it is due to the same dissipation mechanism as in the Bi-2:2:1:2 film.

From the experimental results we conclude that a surface barrier for vortex entry and exit is effective in the Bi-2:2:1:2 films, but is inefficient in the Nb/Cu multilayers. Therefore one might speculate that in Bi-2:2:1:2 the FLL-dissipation maxima at the matching fields are caused by the interaction of the vortices with surface barriers. In the vicinity of the matching fields the flux-line configuration is unstable and the hopping rate for vortices to overcome the surface barrier might be enhanced. This interpretation naturally explains the absence of damping maxima in the Nb/Cu multilayer with outer Cu layers. The observation of only tiny damping maxima in the 200 nm thin Y-1:2:3 film might be due to a corroded surface of that film.

E. Deviations from the simple model

The model of Mawatari and Yamafuji[1] predicts rearrangements of the FLL at constant field intervals ΔB, thus evenly spaced dissipation maxima might be expected. In contrast, the damping of vibrating Bi-2:2:1:2 films generally shows only a few of the expected maxima. The selection rules depend on temperature and angle Θ.

In the model a defect free superconductor is assumed. The Bi-2:2:1:2 film, however, shows strong bulk pinning as can be seen from the $\cos^2\Theta$ variation of the resonance frequency enhancement in Fig. 2. We observed that the damping maxima are most clearly seen in the intermediate temperature range. At low temperatures $T \leqslant 20$ K the formation of an ordered FLL structure is hindered by strong bulk pinning, at high temperatures near the irreversibility temperature $T_{\rm irr}$ thermal fluctuations destroy the FLL order or the coupling between the pancake vortices.

Moreover, beside the formation of a FLL commensurate with the film thickness we expect a matching to the layered structure due to the intrinsic pinning mechanism.[43,44] Oussena *et al.*[45] observed a nonmonotonic dependence of the magnetization of a twin free Y-1:2:3 single crystal in a magnetic field parallel to the CuO_2 planes. Their crystal has a thickness $d_p = 0.125$ mm $\gg \lambda_{ab}$. A similar nonmonotonic variation of the critical current density in Pb-Bi films with a periodic variation of the Bi content was reported by Raffy *et al.*[46] The maxima in the magnetization of the Y-1:2:3 crystal can be understood assuming a matching of the FLL to the layered structure that has a periodicity s, i.e., $a_c = ns$, $n = 1,2,\ldots$.[47] In the case of Bi-2:2:1:2 with $\gamma \simeq 150$ and $s = 15$ Å we obtain the matching fields

$$B_n = \frac{\Phi_0}{\gamma s^2 n^2}, \quad n = 1,2,\ldots . \tag{8}$$

These matching fields B_n are of the same order of magnitude than the matching fields B_N expected from a FLL commensurate to the film surfaces. Qualitatively the suppression of damping maxima at the matching fields B_N can be understood from a competition between the matching to the film thickness and to the layered structure, respectively.

Cooley and Grishin[48] considered a modified critical state model (''terrace critical state'') for a superconducting slab with a regular array of columnar pinning centers with pin lattice constant a_p. In magnetic fields parallel to the columnar pins they found a periodic variation of the magnetization with period $\Delta B \simeq \Phi_0 / a_p^2$. Cooley and Grishin[48] suggest that the model might be applicable to the pinning by a layered structure if $a_p^2 \simeq \lambda_{ab} s$ is substituted. From the superconducting parameters for Bi-2:2:1:2 we estimate a period $\Delta B \simeq 6.9$ T that is much larger than the observed period.

V. CONCLUSIONS

In this work the flux-line dissipation and pinning force of superconducting films has been investigated in magnetic fields that are oriented under a small angle with respect to the sample surface. In a $Bi_2Sr_2CaCu_2O_8$ film a series of pronounced maxima is found in the irreversible region of the magnetic phase diagram, a $YBa_2Cu_3O_7$ film displays only tiny dissipation maxima, whereas no damping peak structure is observed in a Nb/Cu multilayer. We have evaluated the matching fields B_N in the Bi-2:2:1:2 film defined by the dissipation maxima at fixed angle and temperatures $T \leqslant 60$ K. The matching fields observed at a fixed angle are found to be equally spaced with an angle independent separation $\Delta B = 0.7 \pm 0.1$ T at $\Theta = 0°$ and $\Theta = 5°$.

Calculations within the anisotropic London model show that the flux-line lattice parallel to the film surfaces forms a sequence of states, each consisting of N flux-line rows.[1] At well defined field values B_N the FLL rearranges suddenly from $N-1$ to N flux-line rows, whereas the critical current density sustained by the surface displays a minimum. The comparison of the rearrangement fields with the experimentally determined matching fields shows semiquantitative agreement.

This work and the work of Hünnekes *et al.*[10] show that the superheating fields of Bi-2:2:1:2 and Y-1:2:3 films are of the same order of magnitude. We conclude that the stacks of pancake vortices in the investigated Bi-2:2:1:2 film in the angle range $\cot\Theta \ll \gamma$ behave like flux lines in a 3D-anisotropic superconductor. Moreover, since only the pancake vortices in the CuO_2 planes are supposed to cause dissipation,[16] our results show that there is a coupling between the pancake vortices in the field range $B \leqslant 6$ T or $B_\perp \leqslant 0.5$ T. The competition between the commensurability of the FLL to the film surfaces and the layered structure as well as the isotropic bulk pinning might cause the observed deviations from the surface pinning model.

The magnetization of the Nb/Cu multilayer perpendicular to the Nb layers exhibits a series of maxima at magnetic fields B_N that agree with the rearrangement fields of the FLL if the surface barrier for vortex entry is neglected.[8] In contrast, in vibrating reed measurements on the Nb/Cu multilayer no damping peak structure below B_{c2} that indicates FLL rearrangements was found. The surface barriers of the Nb/Cu multilayer are reduced by evaporation of rather thick outer Cu layers. Therefore we propose that the dissipation maxima observed in Bi-2:2:1:2 films and Y-1:2:3 films are due to flux lines hopping over surface barriers.

ACKNOWLEDGMENTS

We wish to acknowledge the collaboration and support of H.F. Braun. We thank B. Ivlev and D. Rainer for valuable discussions. This work was supported by the Graduiertenkolleg ''Low Temperature Physics,'' the Deutsche Forschungsgemeinschaft under Po 88/13 and the Human Capability and Mobility flux pinning program.

APPENDIX: CRITICAL CURRENT DENSITY OF A SUPERCONDUCTING FILM IN A PARALLEL FIELD

In this appendix the equations for the critical current density and the FLL constants of superconducting films in parallel magnetic fields are summarized. Furthermore the critical current density and the FLL constants are derived in the first order in the parameter ξ / d_p. The calculations are performed for an isotropic superconductor. The results are generalized to uniaxially anisotropic superconductors by the following scaling prescription:

$$\lambda \to \gamma^{1/2} \lambda_{ab}, \quad \xi \to \gamma^{-1/2} \xi_{ab}, \quad d_p \to \gamma^{1/2} d_p . \tag{A1}$$

The critical current density that a FLL parallel to a superconducting film is able to sustain due to the interaction with the film surfaces was calculated analytically by Mawatari and Yamafuji.[1] The equations derived in Ref. 1 are summarized here for convenience.

The superconducting film extends in the y-z plane with the film surfaces at $x=0$ and $x=d_p$. The magnetic field $\vec{B}=B\hat{z}$ is oriented along the z axis, the transport current $\vec{J}=J\hat{y}$ along the y axis.

A_x and A_y denote the FLL constants along the thickness of the film and along the flux-line rows, respectively; see inset Fig. 12. If N flux-line rows at positions x_i are present in the film, the averaged position of the flux-line rows along the thickness of the film is $\bar{X}=N^{-1}\Sigma_{i=1}^{N}x_i$. Since the Lorentz force points in the positive x direction, the vortex rows are pushed towards the film surface at $x=d_p$, i.e., $\bar{X}>d_p/2$. In the magnetic field range $B_{(N-1)N}\leqslant B\leqslant B_{NN}$, $N=1, 2, 3, \ldots$, the critical current density $J_c=J_{c,\mathrm{ex}}^{(N)}$ is supplied by the surface barrier for vortex exit out of the film, in the magnetic field range $B_{NN}\leqslant B\leqslant B_{N(N+1)}$, $N=0, 1, 2, \ldots$, the critical current density $J_c=J_{c,\mathrm{en}}^{(N)}$ is determined by the surface barrier for vortex entry into the film. The crossover fields $B_{(N-1)N}$ and B_{NN} denote the boundaries between magnetic field regions belonging to different pinning mechanisms and are determined by requiring the critical current density to be a continuous function of B. The above-mentioned matching fields are given by $B_N=B_{(N-1)N}$, $N=1,2,3,\ldots$.

We choose the following reduced units: $j=J_c/J_{\mathrm{dp}}$, $b=B/B_{\mathrm{sh}}$, $b_{(N-1)N}=B_{(N-1)N}/B_{\mathrm{sh}}$, $b_{NN}=B_{NN}/B_{\mathrm{sh}}$, $a_x=A_x/d_p$, $a_y=A_y/d_p$, $\bar{x}=\bar{X}/d_p$, and $\zeta=\xi/d_p$. $J_{\mathrm{dp}}=\Phi_0/2\sqrt{2}\pi\mu_0\lambda^2\xi$ denotes the depairing current, $B_{\mathrm{sh}}=\Phi_0/\sqrt{2}\pi\xi d_p$ the superheating field, and d_p the film thickness. The model is valid in the limits $(d_p/2\lambda)^2\ll 1$ and $\xi\ll\lambda$.

(1) J_c in the Meissner phase:

$0\leqslant b\leqslant b_{01}$:

$$j_{c,\mathrm{en}}^{(0)}=1-b. \tag{A2}$$

(2) J_c in the presence of one flux-line row:

$$j=\left(b-\sqrt{2}\pi\frac{\zeta}{a_y}\right)(2\bar{x}-1), \tag{A3}$$

$$b\left[\frac{1}{2}-\bar{x}(1-\bar{x})\right]=\frac{\zeta}{\sqrt{2}}\left[\frac{\pi}{a_y}-1+\ln\left(\frac{a_y}{\sqrt{2}\pi\zeta}\right)\right]; \tag{A4}$$

$b_{01}\leqslant b\leqslant b_{11}$: $j_{c,\mathrm{ex}}^{(1)}$ is determined by Eqs. (A3) and (A4) and

$$j=j_{c,\mathrm{ex}}^{(1)}, \tag{A5}$$

$$(2\bar{x}-1)^2=\left(1-\frac{\sqrt{2}\pi\zeta}{ba_y}\right)\left(1-\frac{a_y}{\pi}\right); \tag{A6}$$

$b_{11}\leqslant b\leqslant b_{12}$: $j_{c,\mathrm{en}}^{(1)}$ is determined by Eqs. (A3) and (A4) and

$$j=j_{c,\mathrm{en}}^{(1)}, \tag{A7}$$

$$j_{c,\mathrm{en}}^{(1)}=1-\left[b-2\sqrt{2}\pi\frac{\zeta}{a_y}(1-\bar{x})\right]. \tag{A8}$$

(3) J_c in the presence of N flux-line rows, $N\geqslant 2$:

$$j=b(1-Na_x)(2\bar{x}-1), \tag{A9}$$

$$(2\bar{x}-1)^2=a_x^2-(1-Na_x)^2-\frac{2\sqrt{2}\zeta}{b}[1+\ln(ba_x)], \tag{A10}$$

$$a_xa_y=\frac{\sqrt{2}\pi\zeta}{b}; \tag{A11}$$

$b_{(N-1)N}\leqslant b\leqslant b_{NN}$: $j_{c,\mathrm{ex}}^{(N)}$ is determined by Eqs. (A9)–(A11) and

$$j=j_{c,\mathrm{ex}}^{(N)}, \tag{A12}$$

$$(2\bar{x}-1)^2=(1-Na_x)\left[1-Na_x+\frac{1}{N}\left(a_x-\frac{a_y}{\pi}\right)\right]; \tag{A13}$$

$b_{NN}\leqslant b\leqslant b_{N(N+1)}$: $j_{c,\mathrm{en}}^{(N)}$ is determined by Eqs. (A9)–(A11) and

$$j=j_{c,\mathrm{en}}^{(N)}, \tag{A14}$$

$$j_{c,\mathrm{en}}^{(N)}=1-\left[b-2\sqrt{2}\pi N\frac{\zeta}{a_y}(1-\bar{x})\right]. \tag{A15}$$

The equations (A3)–(A8) and (A9)–(A15) have been solved numerically.

We have obtained a simple analytical solution of the equations (A2)–(A15) in the limit $\xi/d_p\ll 1$.

(1) J_c in the Meissner phase, $\xi/d_p\ll 1$:

$0\leqslant b\leqslant b_{01}$:

$$j_{c,\mathrm{en}}^{(0)}=1-b. \tag{A16}$$

(2) J_c in the presence of one flux-line row, $\xi/d_p\ll 1$:

$b_{01}\leqslant b\leqslant b_{11}$:

$$j_{c,\mathrm{ex}}^{(1)}=\frac{b}{3\sqrt{3}}, \tag{A17}$$

$$a_y=\frac{3\sqrt{2}\pi}{2b}\zeta, \tag{A18}$$

$$\bar{x}=\frac{1}{2}\left(1+\frac{\sqrt{3}}{3}\right); \tag{A19}$$

$b_{11}\leqslant b\leqslant b_{12}$:

$$j_{c,\mathrm{en}}^{(1)}=\left(1-b+b\sqrt{2-\frac{2}{b}}\right)\left(1-\sqrt{2-\frac{2}{b}}\right), \tag{A20}$$

$$a_y=\frac{\sqrt{2}\pi}{2b-1-b\sqrt{2-\frac{2}{b}}}\zeta, \tag{A21}$$

$$\bar{x}=1-\frac{1}{2}\sqrt{2-\frac{2}{b}}\,. \tag{A22}$$

(3) J_c in the presence of N flux-line rows, $N\geqslant 2$, $\xi/d_p\ll 1$:

$b_{(N-1)N}\leqslant b\leqslant b_{NN}$:

$$j_{c,\mathrm{ex}}^{(N)}=b(1-Na_x)(2\bar{x}-1), \tag{A23}$$

$$a_x=\frac{4N^2-1-\sqrt{8N^2+1}}{4N(N^2-1)}, \tag{A24}$$

$$a_y=\frac{\sqrt{2}\pi}{a_x b}\zeta, \tag{A25}$$

$$\bar{x}=\frac{1}{2}[1+\sqrt{a_x^2-(1-Na_x)^2}]; \tag{A26}$$

$b_{NN}\leqslant b\leqslant b_{N(N+1)}$:

$$j_{c,\mathrm{en}}^{(N)}=1-b[1-2Na_x(1-\bar{x})], \tag{A27}$$

$$a_x=\frac{N(2b-1)-\sqrt{2b^2-2b+1-N^2}}{b(2N^2-1)}, \tag{A28}$$

$$a_y=\frac{\sqrt{2}\pi}{a_x b}\zeta, \tag{A29}$$

$$\bar{x}=\frac{1}{2}\left[1+\frac{1-b(1-Na_x)}{b}\right]. \tag{A30}$$

*Present address: Vrije Universiteit Amsterdam, Faculty of Physics and Astronomy, De Boelelaan 1081, 1081 HV Amsterdam, The Netherlands.

†Present address: Department of Superconductivity and Magnetism, University of Leipzig, Linnéstraße 5, D-04103 Leipzig, Germany.

‡Present address: Laboratorium voor Vaste-Stoffysika en Magnetisme, Katholieke Universiteit Leuven, B-3001 Leuven, Belgium.

§Present address: Johannes-Gutenberg-Universität Mainz, Institut für Physik, Staudingerweg 7, D-55099 Mainz, Germany.

[1] Y. Mawatari and K. Yamafuji, Physica C **228**, 336 (1994).

[2] J. Sutton, Proc. Phys. Soc. **87**, 791 (1966).

[3] P. Monceau, D. Saint-James, and G. Waysand, Phys. Rev. B **12**, 3673 (1975).

[4] T. Yamashita and Y. Onodera, Solid State Commun. **13**, 1289 (1973); T. Yamashita and L. Rinderer, J. Low Temp. Phys. **24**, 695 (1976).

[5] N.Ya. Fogel and V.G. Cherkasova, Physica B **107**, 291 (1981).

[6] P. Lobotka, I. Vávra, R. Senderák, D. Machajdïk, M. Jergel, Š. Gaži, E. Rosseel, M. Baert, Y. Bruynseraede, M. Forsthuber, and G. Hilscher, Physica C **229**, 231 (1994).

[7] A. Pruymboom, P.H. Kes, E. van der Drift, and S. Radelaar, Phys. Rev. Lett. **60**, 1430 (1988).

[8] S.H. Brongersma, E. Verweij, N.J. Koeman, D.G. de Groot, R. Griessen, and B.I. Ivlev, Phys. Rev. Lett. **71**, 2319 (1994).

[9] S.H. Brongersma, J.J.M. Pothuizen, E. Verweij, N.J. Koeman, D.G. de Groot, and R. Griessen, J. Alloys Compounds **195**, 443 (1993).

[10] C. Hünnekes, H.G. Bohn, W. Schilling, and H. Schulz, Phys. Rev. Lett. **72**, 2271 (1994).

[11] S.H. Brongersma, B.I. Ivlev, and R. Griessen, Phys. Rev. Lett. **73**, 3329 (1994); C. Hünnekes, H.G. Bohn, W. Schilling, and H. Schulz, *ibid.* **73**, 3330 (1994).

[12] D.E. Farrell, J.P. Rice, D.M. Ginsberg, and J.Z. Liu, Phys. Rev. Lett. **64**, 1573 (1990).

[13] J.C. Martínez, S.H. Brongersma, A. Koshelev, B. Ivlev, P.H. Kes, R.P. Griessen, D.G. de Groot, Z. Tarnavski, and A.A. Menovsky, Phys. Rev. Lett. **69**, 2276 (1992).

[14] L.N. Bulaevskii, M. Ledvij, and V.G. Kogan, Phys. Rev. B **46**, 366 (1992); L.N. Bulaevskii and J.R. Clem, *ibid.* **44**, 10 234 (1991).

[15] D. Feinberg, Physica C **194**, 126 (1992).

[16] P.H. Kes, J. Aarts, V.M. Vinokur, and C.J. van der Beek, Phys. Rev. Lett. **64**, 1063 (1990).

[17] C. Durán, J. Jazyi, F. de la Cruz, D.J. Bishop, D.B. Mitzi, and A. Kapitulnik, Phys. Rev. B **44**, 7737 (1991).

[18] Y. Kopelevich, A. Gupta, and P. Esquinazi, Phys. Rev. Lett. **70**, 666 (1993).

[19] P. Wagner, F. Hillmer, U. Frey, H. Adrian, T. Steinborn, L. Ranno, A. Elschner, I. Heyvaert, and Y. Bruynseraede, Physica C **215**, 123 (1993); P. Wagner, F. Hillmer, U. Frey, and H. Adrian, Phys. Rev. B **49**, 13 184 (1994).

[20] V.V. Lemanov, A.L. Kholkin, and A.B. Sherman, Pis'ma Zh. Eksp. Teor. Fiz. **56**, 580 (1992) [JETP Lett. **56**, 562 (1992)].

[21] M. Ziese, P. Esquinazi, and H.F. Braun, Supercond. Sci. Technol. **7**, 869 (1994).

[22] E.H. Brandt, P. Esquinazi, H. Neckel, and G. Weiss, Phys. Rev. Lett. **56**, 89 (1986); E.H. Brandt, P. Esquinazi, and H. Neckel, J. Low Temp. Phys. **63**, 187 (1986).

[23] R. Labusch, Cryst. Lattice Defects **1**, 1 (1969).

[24] P. Esquinazi, J. Low Temp. Phys. **85**, 139 (1991).

[25] A.P. Malozemoff, T.K. Worthington, Y. Yeshurun, F. Holtzberg, and P.H. Kes, Phys. Rev. B **38**, 7203 (1988).

[26] A. Gupta, P. Esquinazi, H.F. Braun, W. Gerhäuser, H.-W. Neumüller, K. Heine, and J. Tenbrink, Europhys. Lett. **10**, 663 (1989); A. Gupta, P. Esquinazi, H.F. Braun, and H.-W. Neumüller, Phys. Rev. Lett. **63**, 1869 (1989).

[27] A. Gupta, Y. Kopelevich, M. Ziese, P. Esquinazi, P. Fischer, F.I. Schulz, and H.F. Braun, Phys. Rev. B **48**, 6359 (1993).

[28] M. Ziese, P. Esquinazi, Y. Kopelevich, and A.B. Sherman, Physica C **224**, 79 (1994).

[29] C.P. Bean and J.D. Livingston, Phys. Rev. Lett. **12**, 14 (1964).

[30] P.G. de Gennes, Solid State Commun. **3**, 127 (1965).

[31] C. Carter, Can. J. Phys. **47**, 1447 (1969).

[32] S. Takács, Czech. J. Phys. B **33**, 1248 (1983).

[33] J.C. Martinez, P.J.E.M. van der Linden, L.N. Bulaevskii, S.H. Brongersma, A. Koshelev, J.A.A.J. Perenboom, A.A. Menovsky, and P.H. Kes, Phys. Rev. Lett. **72**, 3614 (1994).
[34] R. Jin, A. Schilling, and H.R. Ott, Phys. Rev. B **49**, 9218 (1994).
[35] R. Kleiner, F. Steinmeyer, G. Kunkel, and P. Müller, Phys. Rev. Lett. **68**, 2394 (1992).
[36] W.E. Lawrence and S. Doniach, in *Proceedings of the 12th International Conference on Low Temperature Physics, Kyoto, Japan, 1970*, edited by E. Kanda (Keigaku, Tokyo, 1971), p. 361.
[37] A. Buzdin and D. Feinberg, Phys. Lett. A **165**, 281 (1992).
[38] D. Kumar, M.G. Blamire, R.A. Doyle, A.M. Campbell, and J.E. Evetts, J. Appl. Phys. **76**, 2361 (1994).
[39] C. Hünnekes, Ph.D. thesis, KFA Jülich, 1994.
[40] If it is assumed that B_{c1} is reduced in this film to a value $B_{c1} \leqslant B_1$, one can estimate the matching fields $B_N = 0.25$, 0.45, 0.65, 0.85 T from the value of the first observed matching field $B_1 = 0.25$ T with Eq. (7). The damping of the 43 nm thin Y-1:2:3 film shows artifacts at $B \simeq 0.41$ T and $B \simeq 0.6$ T. Due to these experimental uncertainties the observation of the matching fields B_2 and B_3 might be obscured.
[41] S.H. Brongersma, D.G. de Groot, and R. Griessen, Physica C **235-240**, 2589 (1994).
[42] P.S. Swartz and H.R. Hart, Jr., Phys. Rev. **137**, A818 (1965).
[43] M. Tachiki and S. Takahashi, Solid State Commun. **70**, 291 (1989); **72**, 1083 (1989).
[44] R.A. Doyle, A.M. Campbell, and R.E. Somekh, Phys. Rev. Lett. **71**, 4241 (1993).
[45] M. Oussena, P.A.J. de Groot, R. Gagnon, and L. Taillefer, Phys. Rev. Lett. **72**, 3606 (1994).
[46] H. Raffy, E. Guyon, and J.C. Renard, Solid State Commun. **14**, 427 (1974); **14**, 431 (1974).
[47] S. Ami and K. Maki, Prog. Theor. Phys. **53**, 1 (1975).
[48] L.D. Cooley and A.M. Grishin, Phys. Rev. Lett. **74**, 2788 (1995).